Carbohydrate Polymer Technologies and Applications 6 (2023) 100373

Contents lists available at ScienceDirect

Carbohydrate Polymer Technologies and Applications

journal homepage: www.sciencedirect.com/journal/carbohydrate-polymer-technologies-and-applications

Self-assembled chitosan-sodium usnate drug delivery nanosystems: Synthesis, characterization, stability studies, in vitro cytotoxicity and in vivo biocompatibility against 143 B cells

Benedetta Brugnoli [a], Alessia Mariano [b], Beatrice Simonis [a,c], Cecilia Bombelli [c], Simona Sennato [d], Antonella Piozzi [a], Vincenzo Taresco [e], Veeren M. Chauhan [f], Steven M. Howdle [e], Anna Scotto d'Abusco [b,*], Iolanda Francolini [a,*]

[a] Department of Chemistry, Sapienza University of Rome, 00185, Rome, Italy
[b] Department of Biochemical Sciences, Sapienza University of Rome, P.le A. Moro, 5, 00185, Rome, Italy
[c] CNR-Institute for Biological Systems (ISB), Secondary Office of Rome-Reaction Mechanisms c/o Chemistry Department, Sapienza University, Rome, Italy
[d] CNR- Institute of Complex Systems (ISC) and Sapienza and Physics Department, Sapienza University, Rome, Italy
[e] Department of Chemistry, University of Nottingham, Nottingham, NG7 2RD, UK
[f] School of Pharmacy, Boots Science Building, University of Nottingham, Nottingham, NG7 2RD, UK

ARTICLE INFO

Keywords:
Chitosan nanoparticles
Nano-particle drug delivery systems
Caenorhabditis elegans nematodes
Sodium usnate
143B cells Maspin stimulation
Osteosarcoma

ABSTRACT

Polymers are among the most studied materials as drug carriers, due to their tunable chemical structure and ability to self-assemble to give different types of nanostructures. In this study, chitosan (CS) nanoparticles (NPs) were investigated as carriers for the anticancer drug sodium usnate (NaU) for the treatment of osteosarcoma (OS), which is the most prevalent primary malignant bone sarcoma in pediatric and adolescent patients. CS nano-assembling was induced by electrostatic interactions with the drug and the anionic cross-linker tripolyphosphate, thus obtaining stable nanosystems and a high drug encapsulation efficiency. Importantly, a reduction in NaU hepatotoxicity when encapsulated in CS NPs compared to free NaU was evidenced, suggesting that CS may have a protective role against liver damage. Unfortunately, NaU encapsulation also reduced drug toxicity versus osteosarcoma 143B cells compared to free NaU. Nevertheless, NaU-loaded CS NPs (0.312 mg/mL) were found to decrease 143B cells viability after 48 h and 72 h treatment without being hepatotoxic. Interestingly, this system also stimulated in 143B cells Maspin production, an agent known for its tumor suppressor properties. Relevant synergistic activity between CS and NaU in promoting Maspin stimulation was found. That suggests the potential of the systems to reduce invasiveness of OS cancer.

1. Introduction

Nano-structured drug delivery systems have an outstanding position in the pharmaceutical and medical fields since they can enable the release of the active pharmaceutical ingredient at desired therapeutic doses, improve drug solubility, protect drugs from degradation, and reduce toxic effects (Adepu & Ramakrishna, 2021; Venditti et al. 2020). Synthetic or natural polymers are among the most studied materials as drug carriers, due to their tunable chemical structure and ability to self-assemble to give different unique nanostructures (Cautela et al., 2020; Du et al., 2022; Taresco et al., 2015a; Tasca et al., 2020).

The use of nanomedicines is a breakthrough (Nguyen & Lai, 2022), which has not yet reached full potentialities, leaving a big margin of improvement especially for the treatment of cancer, where it may allow for specific site targeting and side effects decrease (Hare et al., 2017; Rasool et al., 2022).

Osteosarcoma (OS) is the most common primary malignant bone sarcoma which mainly affects pediatric and adolescent patients under 20 (Li et al., 2023). OS involves long bones of the limbs, near the metaphyseal growth plate, and common (femur, tibia and humerus) and less common sites (skull, jaw or pelvis) (Kansara et al., 2014). Even if initially the prognosis of osteosarcoma was very poor, during the last years, the OS prognosis has positively improved, leading to reduction of development of metastases and minimizing last resources strategy as

* Corresponding authors.
E-mail addresses: anna.scottodabusco@uniroma1.it (A. Scotto d'Abusco), iolanda.francolini@uniroma1.it (I. Francolini).

https://doi.org/10.1016/j.carpta.2023.100373

Available online 29 September 2023

amputations, as well as to a prolonged patient survival (Isakoff et al., 2015).

Chemotherapy remains the most used therapeutic strategy against OS (Li et al., 2023). Conventionally, OS is treated before (neoadjuvant) and after (adjuvant) surgery with systemic chemotherapies able to interfere with crucial cellular mechanisms, leading to cellular apoptosis, cellular cycle alteration and inhibition of metastatic process (Lilienthal & Herold, 2020). Unfortunately, chemotherapy causes alterations in cellular growth and differentiations not only in cancerous cells but also in healthy ones (Li et al., 2023). For this reason, it would be useful to develop efficacious therapies against cancer to avoid systemic toxicity, especially for young patients. In addition, chemotherapy leads to practical disadvantages because of drug poor solubility which cause poor bioavailability, so reduced therapeutic effects and in situ low drug release (Kalaydina et al., 2018; Meng, et al. 2022). The development of nanoparticle-based drug delivery systems may help overcoming the above-mentioned issues, as recently demonstrated also for OS treatment (Barani et al., 2021; Chen et al., 2023).

Chitosan (CS) is a widely employed biocompatible polysaccharide for the development of drug formulations, like gels (Kumar et al., 2009), films (Silvestro et al., 2020a), scaffolds for tissue engineering (Francolini et al., 2019a; Silvestro et al., 2020b; Silvestro et al., 2021), and nanoparticles (Mohammed et al., 2017). Nanoparticles (NPs) prepared with CS typically possess positive surface charge and mucoadhesive properties, which enable them to adhere to mucus membranes and release the drug payload in a sustained release manner, thus facilitating both paracellular and transcellular transport of drugs (Nguyen et al., 2023). For these reasons, CS NPs have been successfully applied for various applications in non-parenteral drug delivery for cancer treatment (Ahmad et al, 2022). As far as OS cancer treatment is concerned, copper-loaded CS NPs were shown to enhance the delivering of copper with beneficial effects in OS therapy (Ai et al., 2017). Similarly, poloxamer-modified trimethyl CS nanoparticles loaded with methotrexate showed higher accumulation in cell cytoplasm region and increased cytotoxicity in MG63 cells compared to free drug (Li et al., 2017). In addition, pure CS has been shown to have anticancer properties against several types of cancer, including OS (Abedian et al., 2019; Maleki et al., 2021). Therefore, the conjugation of CS with an anticancer drug could permit a synergistic action in the inhibition of cancer cell viability.

In the present study, CS NPs were investigated as carriers for the sodium salt of usnic acid (UA), a secondary metabolite of lichens, known for its antimicrobial (Francolini et al., 2004) and anticancer (Luzina & Salakhutdinov, 2018) activity. The molecular mechanism of UA antitumor effect has not been fully elucidated and its uses in clinics are limited because of unfavorable physico-chemical properties (poor solubility in water) and hepatotoxicity (Jin et al., 2013; Kwong & Wang, 2020). UA adsorption/encapsulation in nanocarriers has been described as a strategy to modulate drug release kinetics (Lira et al., 2009) and reduce drug hepatotoxicity (da Silva Santos et al., 2006).

In this study, we were interested in reducing drug hepatotoxicity and in investigating drug effects against OS 143B cell alone and when entrapped in CS nanoparticles. Self-assembled CS NPs were obtained by ionotropic gelation method (Pedroso-Santana & Fleitas-Salazar, 2020) and loaded with the sodium salt of usnic acid, sodium usnate (NaU), to enable drug encapsulation in water, without the use of neither organic solvents nor surfactants. The obtained systems were characterized in terms of size, zeta potential, encapsulation efficiency and drug release kinetics. Hepatotoxicity of free and encapsulated NaU was evaluated against HepG2 cells. Osteosarcoma 143B cell viability and ability to produce the tumor suppressor genes regulating Maspin protein, exhibiting suppressing activity against tumor growth and metastasis (Chen & Yates, 2006), were investigated in both untreated and NaU-loaded CS NPs-treated cells. Relevant synergistic activity of CS and NaU in promoting Maspin stimulation in 143B cells was found and never been described before.

2. Materials and methods

2.1. Materials

Chitosan (CS, low molecular weight, CAS number: 9012-76-4, deacetylation ≥75 %, viscosity 1 % w/V in 1 % acetic acid = 20–300 cps), (+)-Usnic acid (UA), sodium hydroxide (NaOH), hydrochloridric acid (HCl) and acetic acid were purchased from Sigma Aldrich (Darmstadt, Germany). Sodium tripolyphosphate (TPP) was obtained by Alfa Aesar. Water for HPLC Plus was bought by Carlo Erba. No additional purification was required because all compounds were of analytical grade.

2.2. Experimental

2.2.1. Preparation of CS nanoparticles

Chitosan nanoparticles were prepared by ionotropic gelation, using TPP as crosslinking agent (Silvestro et al., 2020b). Initially, CS powder was solubilized in acetic acid (2 mg/mL) to a final concentration of 2 mg/mL and left under stirring until total dissolution. Then, the pH was adjusted to 5, adding a few drops of 1 M NaOH. TPP solution (20 mg/mL) was prepared in MilliQ water at 25 °C (pH = 8). Each solution was filtered through a 0.22 μm cellulose acetate (CA, GVS filter technology) and stored at 4 °C prior to use. CS NPs formation occurred adding dropwise, at room temperature (T = 25 °C) and under stirring (89 G-force), different volumes (10 μL, 100 μL and 1000 μL) of TPP (20 mg/mL) to 5 mL of the CS solution (2 mg/mL), such to obtain three CS:TPP molar ratios (1:0.01, 1:0.1 and 1:1). Then, water was added up to a final volume of 6 mL. The suspensions were left under stirring for 30 min. Each sample was stored at 4 °C until use. The obtained samples were called CS:TPPx, where x is the molar ratio between the two (1:0.01, 1:0.1 and 1:1).

2.2.2. Preparation of NaU-loaded nanoparticles

In order to solubilize usnic acid in water, sodium usnate was obtained by solubilizing usnic acid (0.5 g) in 58 mL of NaOH (0.1 M) (8:1 NaOH:UA molar ratio). The sodium usnate was recovered by lyophilization. Specifically, the solution was cooled by liquid N_2 at -196 °C. Then, the frozen cake was fixed to a freeze drying apparatus where the sample was kept under reduced pressure (0.05 Torr) throughout all process to obtain the lyophilized sample. A yellow/brown powder was recovered with a yield of ca. 70 % because part of the material is lost during the reaction with NaOH as unreacted and also due to difficulties to remove freeze-dried sample and transfer it to a working vessel.

CS:NaU nanoparticles were prepared by adding under stirring to a CS solution (5 mL, 2 mg/mL) different amounts of NaU powder (5.61 mg, 11.22 mg and 22.44 mg). In this way, three final NaU concentrations of 5x, 10x and 20x the NaU toxic concentration towards HEPG2 cells (187 μg/mL) were obtained. Samples were called CS:NaUy where y is the NaU concentration (5x, 10x or 20x). Afterwards, 100 μL of TPP solution (20 mg/mL) and 900 μL of water were added in the same conditions of the unloaded CS:$TPP_{1:0.1}$.

2.2.3. Attenuated total reflectance fourier transformed (ATR-FTIR) infrared spectroscopy

ATR-FTIR spectra were recorded by a Nicolet 6700 (Thermo Fisher Scientific, USA) set with a Golden Gate ATR accessory, at a resolution of 4 cm^{-1} and at 200 scans.

2.2.4. Thermogravimetric analysis (TGA)

TGA was carried out by using a Mettler TG50 thermobalance (Mettler Toledo, USA), from 25 to 500 °C at a 10 °C min^{-1} heating rate and under N_2 flow, using ca. 6-7 mg of sample.

2.2.5. Dynamic light scattering (DLS)

Hydrodynamic size and ζ-potential of CS NPs, plain or loaded with

NaU (after filtration, 200 nm), were evaluated by DLS and DELS measurements using a Zetasizer Nano apparatus (Malvern Instruments Ltd.) equipped with a 4 mW HeNe laser source (632.8 nm). All measurements have been thermostat at 25 °C. DLS autocorrelation functions were analyzed by the cumulant method to obtain the mean size and the polydispersity index (PDI) of the samples (Koppel, 1972). Intensity-weighted NNLS algorithm was used to ascertain the features of the size distribution (Lawson & Hanson, 1974). In DELS measurements, phase analysis light scattering (PALS) was employed to obtain the ζ-potential (Tscharnuter, 2001).

2.2.6. Determination of NaU encapsulation efficiency and release study

NaU loaded-CS NPs were centrifuged (15 min, 2100 G-force) and the supernatant was collected in order to determine the unbound NaU by UV−vis spectroscopy (290 nm). The encapsulation efficiency (EE%) and loading capacity (LC %) were calculated using the following equations:

$$EE\ (\%) = \frac{(total\ amount\ of\ drug - \ amount\ of\ unloaded\ drug)}{total\ amount\ of\ drug} \times 100 \quad (1)$$

$$LC\ (\%) = \frac{Drug\ loaded\ amount\ (mg)}{nanoparticles\ weight\ (mg)} \times 100 \quad (2)$$

NaU cumulative release was evaluated by the dynamic dialysis method (D'Souza, 2014; Modi & Anderson, 2013) that involves the physical separation of the drug loaded nanoparticles from the release environment by usage of a dialysis membrane which allows for ease of sampling at periodic intervals. Specifically, a defined amount of NaU-loaded CS NPs water suspension (1.5 mL) was put into a dialysis bag (CUT OFF 3500), which was then immersed in 90 mL of phosphate buffer (PBS) at pH 7.4, in "sink conditions". At predefined times (from 1 to 1440 min), an aliquot (1.5 mL) was taken and analyzed at UV-Vis spectroscopy. The same aliquot of fresh PBS was replaced to maintain a constant volume in the system.

The Korsmeyer-Peppas and Higuchi models were applied to get insight into the release mechanism of NaU from CS NPs.

The Korsemeyer–Peppas model, applicable for the first 60 % of the release of the drug (Tavares et al., 2016), is described by the following equation:

$$\frac{M_t}{M_\infty} = Kt^n$$

where M_t/M_∞ represents the fractional released drug, t is the time, K is the release constant (mostly providing information on structural features of the nanocarriers), and n is the transport exponent (dimensionless), related to the drug release mechanism (Fickian diffusion or non-Fickian diffusion).

The Higuchi model (Siepmann & Peppas, 2011) can be applied when the release is governed by the diffusion (Fick law J = -D ∂C/∂x) and the drug release depends on the square root of time:

$$Q_t = \left(2D\ C_s\ (A - 0.5Cs)^{0.5}\right) t^{0.5}\ or\ Qt = K^H t^{0.5}$$

Where D is the diffusion coefficient, C_s is the drug solubility, A is the drug content for formulation unit, and K_H is the Higuchi dissolution constant.

2.2.7. Stability studies

The colloidal stability over time stability of NaU unloaded (CS:$TPP_{1:0.1}$) and loaded (CS:NaU_{5x}) CS NPs was examined in water at RT for 15 days. Each sample was regularly analyzed by measuring hydrodynamic diameter and ζ-potential by DLS at defined time intervals (1, 3, 9,10, 14 and 15 days).

2.2.8. Atomic force microscopy

Atomic force microscopy (AFM) was performed with a Dimension Icon (Bruker AXS) instrument. AFM images were acquired in air, at room temperature (25 °C) and under ambient conditions, by employing Scan Asyst™ mode, a Bruker-proprietary imaging mode which continuously monitors the quality of the image and self-optimizes the acquisition parameters by using an algorithm which controls the force response curve at every pixel and allows the use of ultra-low imaging forces, protecting soft samples from damage without compromising the image resolution.

RTESP probes (VEECO Probes, US) with a sharp tip (nominal radius $R \leq 8$ nm) have been used. Samples have been deposited on freshly cleaved mica, incubated for 1 min, then rinsed with Milli-Q water, gently flushed with a stream of nitrogen for drying, and analyzed after ≈30 min. Images have been analyzed using the Nanoscope Analysis software v 1.4; images are presented as 3-d false color map of the height sensor channel, obtained after application of 1st order flattening to remove tilt and adjustment of color scale.

2.3. Cell culture

HepG2 cells, a human hepatocarcinoma cell line, obtained from the American Type Culture Collection (HB-8065 ATCC, Rockville, MD, USA) was used as hepatocytes model. Cells were grown in Dulbecco's modified eagle medium Low Glucose (DMEM) (Sigma), supplemented with 10 % fetal bovine serum (FBS) (Gibco, Thermo Fisher Scientific, Waltham, MA, USA) with 1 % penicillin/streptomycin, 1 % L-glutamine and 1 % sodium pyruvate (Gibco), at 37 °C with 5 % CO_2.

Human osteosarcoma cell lines 143B, obtained from the American Type Culture Collection (CRL-8303 ATCC), were used. Cells were cultured in DMEM Glutamax (Gibco) supplemented with 10 % FBS, 1 % penicillin/streptomycin and 1 % sodium pyruvate and 1 % non-essential aminoacids (Gibco), at 37 °C with 5 % CO_2

2.3.1. Cell viability

To assess a potential cytotoxic effect of NaU on HepG2 hepatocarcinoma cells and on 143B osteosarcoma cells, at different concentrations and time points, an MTS (3-[4,5-dimethylthiazol-2-yl]-5-[3-carboxymethoxyphenyl]-2-[4-sulfophenyl]-2H-tetrazolium)-based colorimetric assay was performed (Promega Corporation, Madison, WI, USA). Cells (about 5×10^3 cells per well) were seeded in a 96-well plate in DMEM supplemented with 10 % fetal bovine serum and cultured for 24 h at 37 °C under 5 % CO_2 atmosphere. The day after seeding, culture medium was next replaced and both types of cells were left untreated (CTL) or treated with different concentrations of NaU for 24, 48, and 72 h. After each time point, 100 μL MTS solution was added to the wells. Spectrophotometric absorbance was directly measured at 492 nm after 3 h incubation.

Following the same protocol, the potential cytotoxic effect of CS NPs, with or without NaU at different concentrations for 24, 48 and 72 h, was analyzed, too.

2.3.2. Immunofluorescence

Maspin was visualized by immunofluorescence. $1{,}5 \times 10^4$ 143B cells were seeded and were left untreated (CTL) and treated with NaU, CS NPs with and without NaU for 24 h. After treatments, the cells were fixed with 4 % paraformaldehyde in PBS for 10 min at 4 °C. After washing with PBS, cells were permeabilized with 0.5 % Triton-X 100 in PBS, for 10 min, at room temperature (25 °C), then blocked with 3 % bovine serum albumin (BSA) in PBS for 30 min, at 25°C. Finally, cells were incubated with anti-Maspin mouse monoclonal antibody (Pharmigen) 1:50 for 1 h at 25 °C, after washing with PBS cells were incubated for 1 h at 25 °C with Alexa Fluor 568 donkey anti-mouse antibody 1:400 (Invitrogen, Thermo Fisher Scientific), to stain Maspin in red. Cells were ultimately washed in PBS and incubated with DAPI (Invitrogen, ThermoFisher Scientific, Waltham, MA, USA), to visualize the nuclei. The images were captured by optical microscope Leica DM IL LED, using AF6000 modular Microscope, and analyzed with Leica DM microscope

(Leica Microsystem, Milan, Italy).

2.3.3. Densitometric analysis

The free software ImageJ (https://imagej.nih.gov/ij/) was used to perform the densitometric analysis of Maspin protein expression. For each cell culture condition, the integrated density values of fluorescence obtained in immunofluorescence experiments was considered.

2.3.4. Biocompatibility test on Caenorhabditis elegans nematodes

The cytotoxicity of lead nanoformulations, identified from *in vitro* assay experiments, were investigated by challenging *Caenorhabditis elegans* Bristol N2 nematodes. Experiments were performed by following the ARRIVE guidelines (https://www.nc3rs.org.uk/arrive-guidelines), in accordance with the U.K. Animals (Scientific Procedures) Act, 1986, where nematodes are considered a partial replacement for animal models (https://nc3rs.org.uk/who-we-are/3rs#replacement). *C. elegans* were maintained on nematode growth media (NGM) agar, synchronized (eggs, Day 1, 20 °C) and collected (adults Day 4, 20 °C) with M9 Buffer (Stiernagle, 2006). Adult *C. elegans* were filtered (Merk 20 μm Nylon filter) and washed with M9 buffer solution (50 mL). *C. elegans* were collected and counted ($n > 40$ with three experimental repeats) in each nanoformulation at the two dilutions (1:3 and 1:10) considered, suspended in M9 buffer solution, with 0.1 OD600 of *Escherichia coli* for sustenance. Controls were used for experimental guidance in the form *E. coli* alone (positive control) and absolute ethanol (20 % v/v, negative control). Nematodes were imaged at Time = 24 h upon addition of challenge. All experimental conditions were conducted in triplicate with a minimum of 40 nematodes per challenge. Viability of nematodes was determined according to motile percentage calculations (Chauhan et al., 2013). An absolute indicator of nematode viability was also determined through the observation of progeny production after 24 h (Jacob et al., 2021).

2.3.5. Statistics

All data were obtained from at least three independent experiments and reported as the mean ± standard deviation (SD). Data were statistically analyzed with two-way repeated measures analysis of variance (ANOVA) with Bonferroni's multiple comparison test, using Prism 5.0 software (GraphPad Software, San Diego, CA, USA). P value < 0.05 was considered significant.

3. Results and discussion

UA (Fig. 1A) is a chiral compound produced by lichens as a secondary metabolite. The biological activity of (+)-usnic acid, the right-handed enantiomer, including antibacterial, cytotoxic, and anti-inflammatory activity, has been widely investigated (Araújo et al., 2015).

Specifically, UA exhibits broad-spectrum antimicrobial activity, especially against Gram-positive bacteria, and it has been shown to inhibit the growth of cancer cells, as recently reviewed (Tripathi et al., 2022). Bioadhesive oral films containing *Usnea barbata* dry ethanol extract displayed *in vitro* anticancer activity towards CLS-354 tumor cells and increased cellular oxidative stress and caspase 3/7 activity triggering apoptotic processes in oral cancer cells (Popovici et al., 2022). Similarly, an UA isoxazole derivative induced an endoplasmic reticulum stress response in breast cancer cells that led to cell death (Pyrczak--Felczykowska et al. 2022).

3.1. Drug encapsulation

Several research groups are working on UA encapsulation to control drug release (Battista et al., 2022; Grumezescu et al., 2013; Rauschenbach et al., 2020), including our research group, who developed different UA-loaded nanocarriers based on cationic polymers (Francolini et al., 2013), polyesters (Martinelli et al., 2014; Taresco et al., 2022), magnetic nanoparticles (Taresco et al., 2015b) and liposomes (Francolini et al., 2019b).

Within the framework of broadening the nature of platforms as polymer nanocarriers for UA, in the present study, CS (Fig. 1B) was selected because of its biocompatibility, biodegradability, and chemical reactivity, which make it a promising material for therapeutic and diagnostic applications.

An easy and organic solvent-free preparation method was set up to prepare drug-loaded CS NPs, by using TPP (Fig. 1C) as crosslinking agent and the water-soluble sodium usnate (Fig. 1A), obtained by deprotonation of UA acidic OH groups. Three hydroxyl groups are present in the molecule. The enolic -OH (position 3) has the strongest acidic feature (pKa = 4.4), due to the inductive effect of the keto-group, and is the most probable to be deprotonated in basic environment (Ingólfsdóttir, 2002).

Three different CS:TPP molar ratios (1:0.01, 1:0.1 and 1:1) were investigated to obtain crosslinked-CS NPs by ionic gelation. Upon addition of TPP into the CS solution, an increase in turbidity was observed (Figure S1A, Supporting Info), suggesting the formation of a colloidal system. DLS analysis evidenced a decrease in CS size after crosslinking with TPP (Table 1), suggesting the formation of nanosized supramolecular assemblies induced by electrostatic interactions. DLS curves are reported in SI (Figure S1B). A general increase in NP size was observed with the increase in TPP amount, suggesting partial aggregation of the systems. That was especially evident for CS:$TPP_{1:1}$ which also formed a suspension not stable over time (Figure S1A, Supporting Info).

The lowest PDI was observed for the CS:$TPP_{1:0.1}$ sample, thus evidencing the formation of a more uniform population of colloidal particles. The DLS trace of CS:$TPP_{1:0.1}$ shows a single peak (Figure S1B). In contrast, the DLS traces of CS:$TPP_{1:0.01}$ and CS:TPP1:1 samples

Table. 1
Size and polydispersity index (PDI), obtained by DLS cumulant analysis and potential, of chitosan and CS:TPPx NPs. Data represent the mean ± standard deviation on three series of repeated measurements.

Sample	Hydrodynamic diameter (nm)	PdI	ζ-potential (mV)
CS	493.0 ± 44.6	0.58 ± 0.02	+ 22.4 ± 1.8
CS:$TPP_{1:0.01}$	92.8 ± 1.8	0.61 ± 0.01	+ 20.7 ± 0.3
CS:$TPP_{1:0.1}$	117.2 ± 1.3	0.23 ± 0.01	+ 17.7 ± 1.4
CS:$TPP_{1:1}$	165.9 ± 86.8	0.56 ± 0.10	+ 26.7 ± 2.1

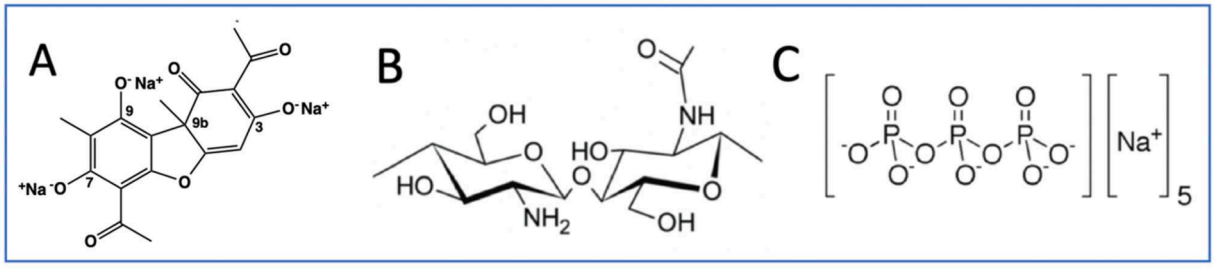

Fig. 1. Chemical structures of sodium usnate (A), chitosan (B) and sodium tripolyphosphate (C).

showed a multimodal distribution sizes with two peaks as a consequence of either weak ability of self-assembling or low stability. Therefore, CS:TPP 1:0.1 ratio was chosen for the experiments of drug encapsulation and further characterization.

The ATR-FTIR spectroscopy was used to investigate the occurrence of CS/TPP electrostatic interactions (Bhumkar & Pokharkar, 2006). In the ATR-FTIR spectrum of the pure CS (Fig. 2), the primary adsorption are: the stretching vibrations of the -OH and -NH groups, which fall between 3600 and 3000 cm^{-1}; the C-H stretching, which falls between 2980 and 2875 cm^{-1}; a peak at 1650 cm^{-1} attributed to the acetylate groups (amide I), a peak at 1570 cm^{-1}ascribed to the N–H bending of primary amines (amide II); an absorption peak at 1419 cm^{-1}associated to $-CH_2$ bending; methyl C-H symmetrical bending at 1377 cm^{-1}; a peak at 1320 cm^{-1} related to the C–N stretching; the absorption peaks in the spectral range from 1150 to 1000 cm^{-1} can be attributed to C-O-C and C-O-H stretching and the peak at 896 cm^{-1} to the C-O-C pyranose ring stretching. In the ATR-FTIR spectrum of the pure TPP the following adsorption are present: 1211 cm^{-1} which is relative to the P=O stretching; 1135 cm^{-1} attributed to the symmetric and antisymmetric stretching of $-PO_2$; 1092 cm^{-1} attributed to the symmetric and antisymmetric stretching of the PO_3 group, and 881 cm^{-1} recognized as the antisymmetric stretching of the P-O-P bond.

The CS:$TPP_{1:0.1}$ NPs exhibited a broad band from 3650 to 2810 cm^{-1} presumably due to the development of intra- and intermolecular hydrogen bonds (Fig. 2). Two intense absorption peaks at 1552 and 1410 cm^{-1} were present and a decrease in the intensity of the peak at 1650 cm^{-1} was observed and related to the interactions of the CS -NH groups with the phosphoric ions of TPP (Bhumkar & Pokharkar, 2006).

3.2. *In vitro cytotoxicity of free sodium usnate against HepG2 cells and 143 cells*

UA and its derivatives are molecules known for decades for different therapeutic properties that have made them the subject of *in vitro* and *in vivo* several studies over the years (Krajka-Kuźniak et al., 2021; Oh, et al., 2022; Wang et al., 2022; Yang et al. 2016). Although the mechanism responsible for UA toxicity is not yet fully established, several studies have shown an uncoupling of oxidative phosphorylation in liver of animal models, which can produce hepatocyte lysis and apoptosis and induce acute liver lesions after treatment with UA (Kwong & Wang, 2020).

Here, the hepatotoxicity of NaU against HepG2 cells, a model of hepatocytes, was investigated to find out the amount of NaU to entrap into the obtained colloidal system CS:$TPP_{1:0.1}$. The viability of HepG2 cells was evaluated following treatments with increased concentrations (1.5, 0.75, 0.375, 0.187, 0.093 and 0.047 mg/mL) of NaU. As it can be observed in Fig. 3, NaU exhibited a significant hepatotoxicity against HepG2 cells at a final concentration of 1.5, 0.75 and 0.375 mg/mL after all the analyzed times, decreasing the percentage of living cells under 50 %. It showed a sub-hepatotoxic effect at 0.187 mg/mL, mainly after 48 h and 72 h of treatment, while at final concentration of 0.093 mg/mL it was not observed a cell viability decrease after 24 h and 48 h treatment and a no significant decrease after 72 h. Finally, at final concentration of 0.047 mg/mL no significant decrease of cell viability was reported after any analysed time. Although a very slight decrease (89.9 % compared to untreated cells) was observed after 48 hours, no decrease was observed after 72 hours. It is reasonable to speculate that these minor fluctuations may be attributed to experimental variability or that after 72 h the cells have responded to NaU insult restoring their viable functions.

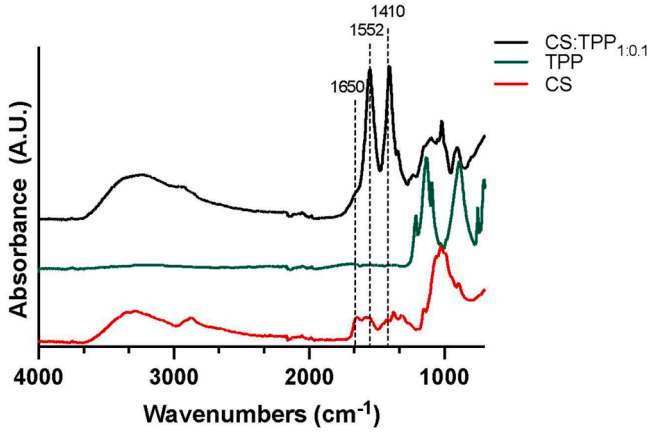

Fig. 2. ATR-FTIR spectra of CS, TPP and CS:$TPP_{1:0.1}$ nanoparticles.

Based on these results, the three NaU concentrations with lower hepatotoxic effect, 0.187, 0.093 and 0.047 mg/mL, were tested on osteosarcoma 143B cells, too. The highest tested concentration (0.187 mg/mL) resulted able to significantly decrease 143B cell viability already at 24 h. Interestingly, also 0.093 and 0.047 mg/mL NaU resulted able to interfere with 143B cell viability after 72 h of treatment, suggesting a cytotoxic activity against the tumor proliferation after a prolonged treatment.

3.3. *Evaluation of encapsulation and release study of NaU*

Accordingly to findings of *in vitro* cytotoxicity tests, NaU concentrations greater than 0.187 mg/mL (the lowest concentration of NaU at which cytotoxicity was observed for both HepG2 and 143B cells) were used for NaU encapsulation into the CS:$TPP_{1:0.1}$ nanoparticles, with the aim to reduce NaU hepatotoxicity still maintaining its effect on osteosarcoma growth. Specifically, three concentrations, 5x, 10x and 20x of the NaU effective concentration (0.187 mg/mL), were used in the encapsulation experiments. The drug was dissolved in water together with CS and the formation of polymer nanostructures was induced by crosslinking with TPP. After TPP addition, only the sample CS:NaU_{5x} formed a stable suspension. In contrast, the samples loaded with higher NaU concentrations, CS:NaU_{10x} and CS:NaU_{20x}, precipitated soon after the preparation. Presumably, CS precipitation occurred at high NaU concentration, caused by pH increase of the solution upon addition of NaU. Indeed, the closer the solution pH to the CS pKa (6.5), the greater the tendency for polymer precipitation (Körpe et al., 2014).

The suspension of the CS:NaU_{5x} sample which did not show precipitation was further characterized. Analysis of size distribution obtained by DLS measurements (Fig. 4A) confirmed the presence of an homogeneous population of nanoparticles and evidenced only slight increase in nanoparticle diameter compared to the blank sample as a consequence of NaU encapsulation. The PDI remained pretty much unchanged (0.23 vs. 0.26) (Table S1, supporting info).

Thermal stability of CS:$TPP_{1:0.1}$ and CS:NaU_{5x} was also investigated by thermogravimetric analysis (Fig. 4B). In all curves, the first step of weight loss between 25–100 °C is attributable to the absorbed water, around 12–13 % in each sample. In the CS curve, the degradation step from 190 to 330 °C was assigned to dehydration of the saccharide rings, depolymerization and decomposition of the acetylated and deacetylated units of the polymer. The temperature of CS degradation increased up to 340–400 °C when crosslinked with TPP (CS:$TPP_{1:0.1}$), thus confirming the formation of ionic interactions between the two components. A further increase in the polymer degradation temperature up to ca. 480 °C was observed when NaU was also present, suggesting that also the drug contributed to polymer assembling. Indeed, NaU can establish multipoint acidic-base interactions with the CS amino groups of CS, stabilizing the structure. Also, the formation of stacking interactions among NaU aromatic groups can contribute to the thermal stabilization of the system.

3.4. *NaU Encapsulation*

NaU Encapsulation Efficiency (EE%) was found to be (61 ± 3) %

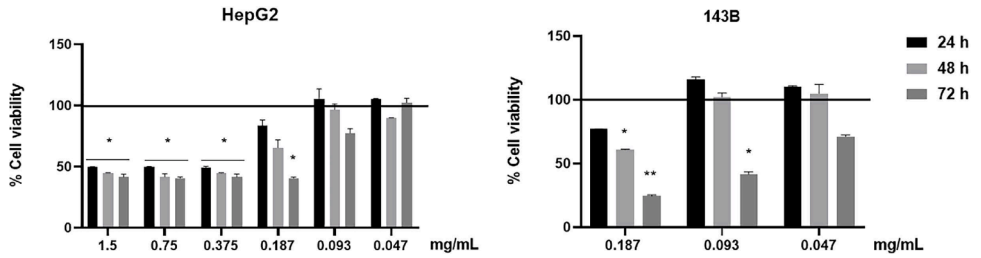

Fig. 3. Cell viability was assessed by the MTS colorimetric method. The viability of HepG2 and 143B cells treated with increased concentrations of NaU after 24, 48 and 72 h. Cell viability of samples was normalized to the untreated cells which is reported as 100 % and represented by a horizontal line. Results are expressed as mean ± Standard Deviation of data obtained by three different experiments. Statistical significance was * $p < 0.05$; ** $p < 0.01$ vs untreated cells.

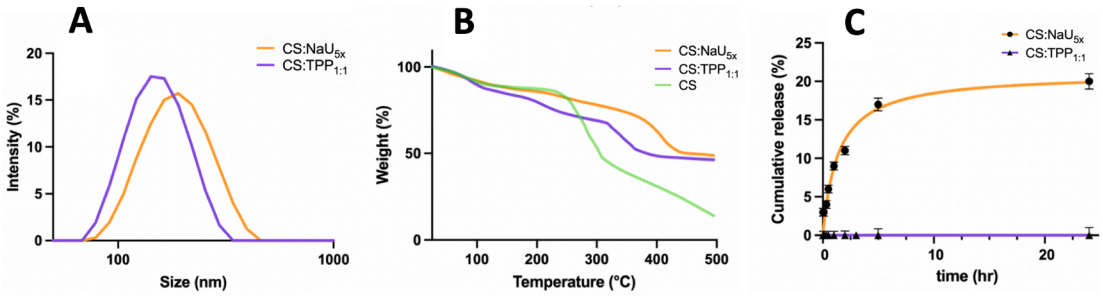

Fig. 4. Intensity-weighted size distribution obtained by NNLS analysis of DLS data (A), thermogravimetric analysis (B) and cumulative NaU release (C) for CS:$TPP_{1:0.1}$ and CS:NaU_{5x}.

from which a loading capacity of 23 % (23 mg of NaU per mg of CS NPs) can be estimated (Table S2, supporting info). The found EE% and LC% values are significantly higher than those reported in the literature for antimicrobial UA-CS NPs obtained by dissolving the drug in a water/DMSO mixture (Khan et al., 2020). Presumably, the herein employed drug encapsulation method, which involved previous deprotonation of the acidic groups of UA, promoted drug affinity and interaction with CS (Dimiou et al., 2023).

In vitro drug release study, performed in PBS pH 7.4 at room temperature (25 °C), showed that only ca. 20 % of the entrapped drug was released in 24 h (Fig. 4C). This finding reflects a drug adsorption throughout specific physico-chemical drug/polymer interactions, which limited drug release. In order to study the release mechanism, the cumulative drug release was fitted by the Korsmeyer-Peppas model (Fig. S2, Supporting Info). In general, according to this model, the release can be considered diffusion-controlled, Fickian mechanism of release (Case I diffusional), for n = 0.45 (Ritger & Peppas, 1987), anomalous (non-Fickian) for $0.45 < n < 0.89$ and a Case II transport (polymer relaxation- or swelling-controlled mechanism) for n = 0.89. For n = 0.9, drug release is controlled by polymer swelling and erosion.

In our case, the transport exponent (n) was found to be 0.34 describing a mechanism of release controlled by drug diffusion within the system. The Higuchi model confirmed a diffusional release mechanism since the linear regression of the release data vs. the root square of time was good ($R^2 = 0.98$, Fig. S2 Supporting Info). However, the very low released amount at the equilibrium suggests that just a small fraction of the entrapped drug, presumably the one adsorbed on the NP surface or weakly interacting with CS, is able to diffuse trough the polymer matrix. In contrast, the majority of the encapsulated drug amount cannot diffuse presumably because of the establishment of strong ionic interactions with CS.

Overall, we can hypothesize that, in our system, cellular internalization of the drug will be mediated by interaction of CS NPs with the cell membrane, and this can overcome the poor water solubility of the drug. In general, positively charged CS NPs displayed enhanced intracellular uptake compared to negatively charged NPs (Dyawanapelly et al., 2016). CS can adhere to the negatively charged biological membranes by electrostatic interaction, promoting cell endocytosis (Dou et al., 2019). CS has been also reported to be able to open the tight junction between epithelial cells, thereby enhancing the permeability of carried drugs (Sheng et al., 2015).

3.5. Stability studies and AFM observations

Stability studies were also performed on plain and loaded nanoparticles within time (from 1 to 15 days) at 25 °C by determining the hydrodynamic diameter and ζ-potential (Fig. 5). Plain CS NPs showed an increase in hydrodynamic size over time suggesting aggregation of the systems. In contrast, the NaU loaded-CS NPs (CS:NaU_{5x}) showed stable values of hydrodynamic diameter and ζ-potential over time. This finding is in agreement with the TGA results, further suggesting that the electrostatic interactions between the drug and polymer contribute to the stabilization of the nanosystems.

Also, AFM observations confirm such hypothesis (Fig. 6).

The empty nanoparticles (Fig. 6A) exhibit a somewhat indistinct

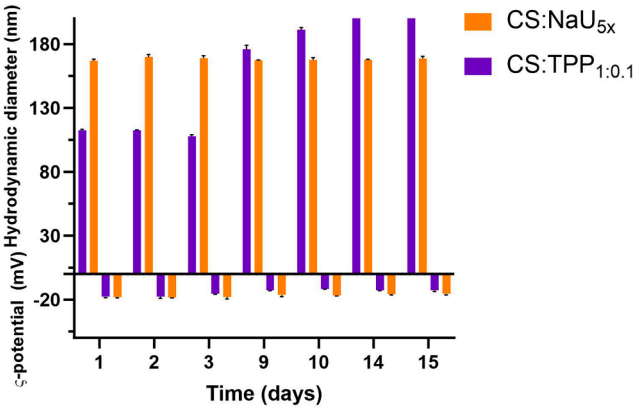

Fig. 5. CS:$TPP_{1:0.1}$ and CS:NaU_{5x} stability over time, evaluated by measurements of hydrodynamic diameter and ζ-potential from day 1 to day 15.

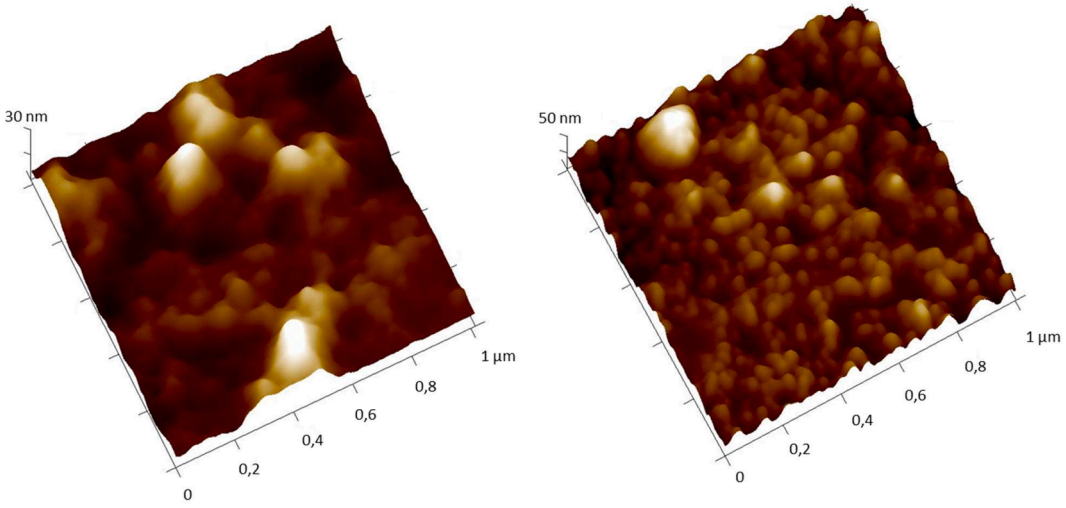

Fig. 6. AFM: 3D topographical images of CS:$TPP_{1:0.1}$ (A) and CS:NaU_{5x} (B) nanoparticles.

appearance, as though they have spread across the substrate or formed interconnections with each other, thereby complicating the identification of individual nanoparticles (Fig. 6B). Conversely, the CS:NaU_{5x} nanosystems display a distinct, more defined spherical morphology. This suggests that the interactions between the drug and polymer prevent the favorable interaction of the positively charged CS with the negatively charged hydrophilic mica substrate.

3.6. *In vitro cytotoxicity of CS NPs with and without NaU*

In order to investigate the advantages in terms of hepatotoxicity and tumor growth of the NaU encapsulation in CS NPs, MTS assay was performed. Both HepG2 and 143B cells were treated with CS:$TPP_{1:0.1}$ and CS:NaU_{5x} diluted to 1:3, 1:10 and 1:50 in cell culture medium, for 24 h, 48 h and 72 h. The dilutions corresponded to 0.312, 0.093 and 0.019 mg/mL NaU concentrations, which are higher and lower than the first toxic concentration of the free NaU (0.187 mg/mL). The investigation of NaU concentrations lower than the toxic concentration of the free NaU aimed at studying the potential effect of NaU on tumor suppressor patterns, like Maspin production, otherwise not achievable in case of significant cell death.

Interestingly, under these experimental conditions, no detrimental effect was observed on HepG2 cells by CS:NaU_{5x} at any analyzed concentration and time (Fig. 7). A significant reduction of NaU hepatotoxicity was obtained when NaU was encapsulated in CS NPs compared to free NaU, obtaining the HepG2 cell cellular viability at the same level of untreated cells. That suggested the protective role of CS against liver damage. Empty CS nanoparticles (CS:$TPP_{1:0.1}$) also resulted not hepatotoxic (Figure S3, Supporting Info).

On the other hand, not statistically significant decrease in cellular viability was obtained after 48 h and 72 h of 143B cell treatment with the 1:3 dilution of CS:NaU_{5x} (0.312 mg/mL), indicating a maintained cytotoxic effect on osteosarcoma cells. However, the CS:NaU_{5x} showed a reduced cytotoxicity compared to the not encapsulated NaU.

3.7. *Assessment of Maspin protein production in OS 143B cells*

Maspin protein (Mammary Serine Protease Inhibitor), a non-inhibitory member of the serine protease family (SerpinB5), has been described as a tumor suppressor molecule in many types of cancer, among them the osteosarcoma (Bodenstine et al., 2012). Maspin has been shown to be able to induce apoptosis, decrease cell proliferation, inhibit metastasis, angiogenesis and invasiveness (Bodenstine et al., 2012). To evaluate the anti-tumor activity of NaU, both free and loaded into CS NPs, in 143B osteosarcoma cells, its ability to stimulate Maspin production was analyzed. Cells were treated with CS:$TPP_{1:0.1}$, CS:NaU_{5x} suspensions, both 1:3 diluted (0.312 mg/mL), and free NaU.

Findings showed that free NaU was not able to stimulate Maspin

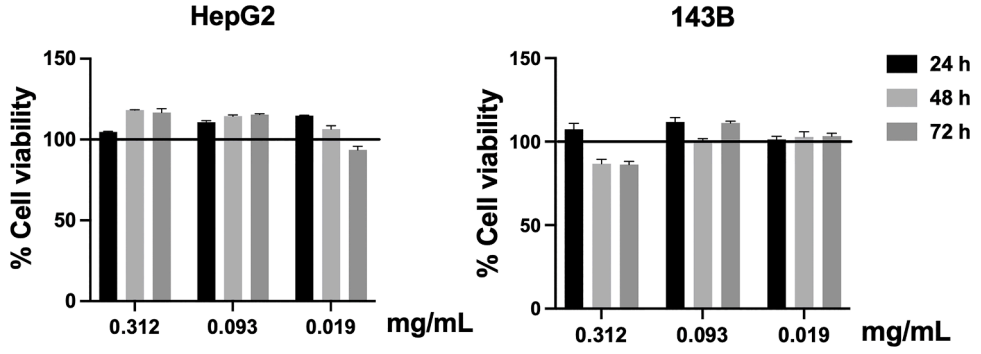

Fig. 7. Cell viability of CS:NaU_{5x} at three dilutions, assessed by the MTS colorimetric method. The viability of HepG2 and 143B cells treated with 1:3 (0.312 mg/mL), 1:10 (0.093 mg/mL) and 1:50 (0.019 mg/mL) dilutions of CS:NaU_{5x} suspensions, after 24, 48 and 72 h. Cell viability of samples was normalized to the untreated cells which is reported as 100 % and represented by a horizontal line. Results are expressed as mean ± SD of data obtained by three different experiments.

production, the expression level, highlighted by red staining measured by ImageJ, was slightly lower compared to level of this protein in untreated cells (Fig. 8). In contrast, both CS:$TPP_{1:0.1}$ and CS:NaU_{5x} stimulate Maspin production, with CS:NaU_{5x} being more effective with respect to CS:$TPP_{1:0.1}$, and only CS:NaU_{5x} was able to significantly stimulate production both in total and nuclear fraction ($^*p < 0.05$) (Fig. 8).

Although chitosan has been reported to have anticancer activity against osteosarcoma (Abedian et al., 2019; Maleki Dana et al., 2021), the ability to stimulate Maspin production has never been shown. The increase of Maspin, which can contrast metastasis and invasiveness of cancer, can be considered a very promising result. Moreover, the ability of CS to potentiate NaU activity in promoting Maspin stimulation, alongside with the decrease of its hepatotoxicity, suggest that the encapsulation of the cytotoxic NaU in CS NPs is an encouraging challenge in oncology therapy strategies. Furthermore, the nuclear localization of Maspin has been found to be a good prognostic factor in cancer fighting (Machowska et al. 2014). Intriguingly, after treatment with both CS:$TPP_{1:0.1}$ and CS:NaU_{5x}, the Maspin localization resulted to be increased into the nuclei. This is a further confirmation of the beneficial effect of NaU encapsulation in CS NPs.

3.8. *In vivo biocompatibility*

C. elegans has been previously adopted as a simple and powerful *in vivo* model to more complex biological systems, such as humans, for the optimization of nano-formulation systems for drug delivery applications (Al-Natour et al., 2020).

On this basis, four CS formulations, 1:3 CS:$TPP_{1:0.1}$, 1:10 CS:$TPP_{1:0.1}$, 1:3 CS:NaU_{5x} (0.312 mg/mL) and 1:10 CS:NaU_{5x} (0.093 mg/mL), appeared stable, with no appearance of any aggregate after 24 h when suspended in M9. All formulations, except *C. elegans* with challenged with ethanol (20 % v/v) did not exhibit significant changes in *C. elegans* viability, measured as a function of nematode motility as well as the production of progeny over the 24 h experimental challenge ($p > 0.05$, Fig. 9 and Supporting Info Video).

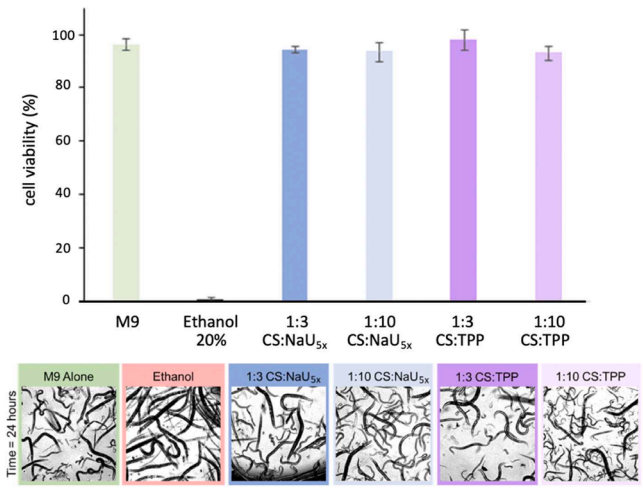

Fig. 9. Up) *C. elegans* viability, as a function of motility, after 24 h challenge with CS formulations, CS:TPP1:0.1 and CS:NaU5x at two dilutions 1:3 (0.312 mg/mL) and 1:10 (0.093 mg/mL). Experiments were conducted in triplicate per formulation with >40 nematodes per experiment, no significant differences in viability were observed, except for those nemtodes treated with ehtanol 20 % v/v ($p > 0.05$) **Down)** Microscope images of nematodes after exposure to polymer NPs. Nematode progeny was observed control maintenance M9 alone and CS treated suspensions after 24 h of exposure, indicative of nematode viability. Progeny were not observed for nematodes treated with ethanol 20 % v/v. See supporting video X for confirmation of nematode motility as an indicator of viability.

Nematodes challenged with absolute ethanol (20 % v/v) were non-motile and did not produce progeny and were therefore considered non-viable Therefore, all the formulations appeared to demonstrate *in vivo* biocompatibility after a 24 h challenge, validating these systems as suitable nano-devices to deliver a toxic active ingredient, such as UA, with minimal toxic side effects on whole organism systems, such as nematodes.

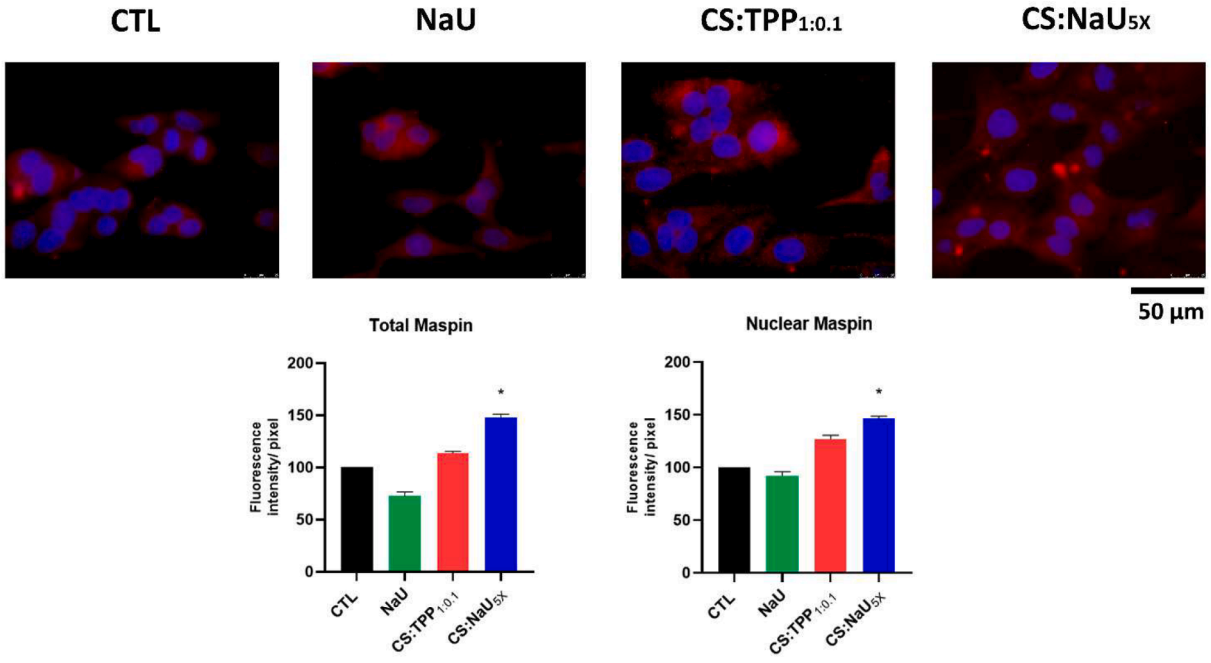

Fig. 8. Effects of free NaU, CS:$TPP_{1:0.1}$ and CS:NaU_{5x} on Maspin protein production. Cells were treated with CS:$TPP_{1:0.1}$ and CS:NaU_{5x} suspensions (1:3 dilution, 0.312 mg/mL) and free NaU (0.312 mg/mL), for 24 h and then analyzed by immunofluorescence using anti-Maspin primary antibody and Alexa Fluor 568 (red) secondary antibody. Nuclei were stained in blue with DAPI (original magnification 63X). The pixel intensities were measured in 20 areas of the images by ImageJ, the results reported in the bottom part of the figure, represent the as mean ± SD of all the 20 measures. Statistical significance was * $p < 0.05$ vs untreated cells.

4. Conclusions

In summary, we have demonstrated that it is possible to reduce the hepatotoxicity of sodium usnate, the sodium salt of usnic acid, by its encapsulation in chitosan nanoparticles. Notably, our study distinguishes itself through a methodology for nanoparticle production that omits the use of organic solvents entirely. Strong drug/polymer interactions were established, as suggested by the increased thermal and colloidal stability of the NaU-loaded NPs (CS:NaU_{5x}) compared to the unloaded NPs. Such good drug/polymer affinity was responsible for the high encapsulation efficiency achieved and also justifies the low drug amount released in 24 h. A reduction in NaU hepatotoxicity when encapsulated in CS NPs compared to free NaU was evidenced, suggesting that CS may have a protective role against liver damage. Unfortunately, NaU encapsulation also reduced drug toxicity versus osteosarcoma 143B cells compared to free NaU. Nevertheless, the 1:3 dilution of CS:NaU_{5x} (0.312 mg/mL) was found to decrease 143B cells viability after 48 h and 72 h treatment without being hepatotoxic. Interestingly, this dilution also stimulated Maspin production in 143B cells and a relevant synergistic activity between CS and NaU in promoting Maspin stimulation was found. Further, the experiments in this study provide validation on the application of *C. elegans* nematodes as a model organism to determine the biocompatible of next generation drug delivery vehicles. The safety of the developed NaU-loaded CS nanoparticles observed in *in vivo* biocompatibility tests further validates these systems as suitable nanoformulations to deliver toxic anticancer agents. Our novel discovery pertaining to the collaborative effect of CS and NaU in stimulating Maspin expression within 143B osteosarcoma cells represents a groundbreaking contribution so far unreported. The advantage of using CS as a drug delivery system is also related to its demonstrated ability to increase drug bioavailability *in vitro* and *in vivo* (Bowman & Leong, 2006; Sharma et al., 2019; Wang et al., 2016). The absorption-promoting effect of CS has been related to the combination of mucoadhesion and the transient opening of tight junctions in the mucosal cell membrane (Wang et al., 2016). In addition, CS nanospheres have been shown to be suitable for drug delivery in the gastrointestinal, ophthalmic, nasal, sublingual, transdermal, vaginal tract, intra-tumoral and oral administration (Bolhassan et al., 2014; Guadarrama-Escobar et al, 2023). Overall, considering the potentiality of the developed system to mitigate the invasiveness of this particular cancer, a promising avenue for future application could involve its integration into combination therapy alongside other anticancer drugs

CRediT authorship contribution statement

Benedetta Brugnoli: Formal analysis, Investigation. **Alessia Mariano:** Formal analysis, Investigation. **Beatrice Simonis:** Formal analysis. **Cecilia Bombelli:** Data curation, Writing – review & editing. **Simona Sennato:** Data curation, Writing – review & editing. **Antonella Piozzi:** Data curation, Writing – review & editing. **Vincenzo Taresco:** Methodology, Data curation, Writing – review & editing. **Veeren M. Chauhan:** Formal analysis, Investigation. **Steven M. Howdle:** Data curation. **Anna Scotto d'Abusco:** Conceptualization, Methodology. **Iolanda Francolini:** Conceptualization, Methodology, Writing – original draft, Funding acquisition.

Declaration of Competing Interest

The authors declare that they have no known competing financial interests or personal relationships that could have appeared to influence the work reported in this paper.

Data availability

The data that supports this study is available from the authors upon reasonable request.

Acknowledgement

This work was supported by the Sapienza University of Roma (Project n. RP12117A5C501A93). VT and VMC would like to thank the University of Nottingham for their Nottingham Research Fellowship.

Supplementary materials

Supplementary material associated with this article can be found, in the online version, at doi:10.1016/j.carpta.2023.100373.

References

Abedian, Z., Moghadamnia, A. A., Zabihi, E., Pourbagher, R., Ghasemi, M., Nouri, H. R., Tashakorian, H., & Jenabian, N. (2019). Anticancer properties of chitosan against osteosarcoma, breast cancer and cervical cancer cell lines. *Caspian Journal of Internal Medicine, 10*(4), 439–446. https://doi.org/10.22088/cjim.10.4.439

Adepu, S., & Ramakrishna, S. (2021). Controlled drug delivery systems: Current status and future directions. *Molecules, 26*(19), 5905. https://doi.org/10.3390/molecules26195905

Ahmad, M. Z., Rizwanullah, Md., Ahmad, J., Alasmary, M. Y., Akhter, Md. H., Abdel-Wahab, B. A., Warsi, M. H., & Haque, A. (2022). Progress in nanomedicine-based drug delivery in designing of chitosan nanoparticles for cancer therapy. *International Journal Of Polymeric Materials And Polymeric Biomaterials, 71*(8), 602–623. https://doi.org/10.1080/00914037.2020.1869737

Ai, J.-w., Liao, W., & Ren, Z.-L. (2017). Enhanced anticancer effect of copper-loaded chitosan nanoparticles against osteosarcoma. *RSC Advances, 7*, 15971–15977. https://doi.org/10.1039/C6RA21648J

Al-Natour, M. A., Yousif, M. D., Cavanagh, R., Abouselo, A., Apebende, E. A., Ghaemmaghami, A., Kim, D. H., Aylott, J. W., Taresco, V., Chauhan, V. M., & Alexander, C. (2020). Facile dye-initiated polymerization of lactide-glycolide generates highly fluorescent poly(lactic-*co*-glycolic acid) for enhanced characterization of cellular delivery. *ACS Macro Letters, 9*(3), 431–437. https://doi.org/10.1021/acsmacrolett.9b01014

Araújo, A. A., de Melo, M. G., Rabelo, T. K., Nunes, P. S., Santos, S. L., Serafini, M. R., Santos, M. R., Quintans-Júnior, L. J., & Gelain, D. P. (2015). Review of the biological properties and toxicity of usnic acid. *Natural Product Research, 29*(23), 2167–2180. https://doi.org/10.1080/14786419.2015.1007455

Barani, M., Mukhtar, M., Rahdar, A., Sargazi, S., Pandey, S., & Kang, M. (2021). Recent advances in nanotechnology-based diagnosis and treatments of human osteosarcoma. *Biosensors, 11*(2), 55. https://doi.org/10.3390/bios11020055

Battista, S., Köber, M., Bellio, P., Celenza, G., Galantini, L., Vargas-Nadal, G., Fagnani, L., Veciana, J., Ventosa, N., & Giansanti, L. (2022). Quatsomes Formulated with l-Prolinol-Derived Surfactants as Antibacterial Nanocarriers of (+)-Usnic Acid with Antioxidant Activity. *ACS Applied Nano Materials, 5*(5), 6140–6148. https://doi.org/10.1021/acsanm.1c04365

Bhumkar, D. R., & Pokharkar, V. B. (2006). Studies on effect of pH on cross-linking of chitosan with sodium tripolyphosphate: a technical note. *AAPS PharmSciTech, 7*(2), E50. https://doi.org/10.1208/pt070250

Bodenstine, T. M., Seftor, R. E., Khalkhali-Ellis, Z., Seftor, E. A., Pemberton, P. A., & Hendrix, M. J. (2012). Maspin: molecular mechanisms and therapeutic implications. *Cancer Metastasis Reviews, 31*(3-4), 529–551. https://doi.org/10.1007/s10555-012-9361-0

Bolhassani, A., Javanzad, S., Saleh, T., Hashemi, M., Aghasadeghi, M. R., & Sadat, S. M. (2014). Polymeric nanoparticles: potent vectors for vaccine delivery targeting cancer and infectious diseases. *Human Vaccines & Immunotherapeutics, 10*, 321–332. https://doi.org/10.4161/hv.26796

Bowman, K., & Leong, K. W. (2006). Chitosan nanoparticles for oral drug and gene delivery. *International Journal of Nanomedicine, 1*(2), 117–128. https://doi.org/10.2147/nano.2006.1.2.117

Cautela, J., Stenqvist, B., Schillén, K., Belić, D., Månsson, L. K., Hagemans, F., Seuss, M., Fery, A., Crassous, J. J., & Galantini, L (2020). Supracolloidal Atomium. *ACS Nano, 14*(11), 15748–15756. https://doi.org/10.1021/acsnano.0c06764

Chauhan, V. M., Orsi, G., Brown, A., Pritchard, D. I., & Aylott, J. W. (2013). Mapping the pharyngeal and intestinal pH of *Caenorhabditis elegans* and real-time luminal pH oscillations using extended dynamic range pH-sensitive nanosensors. *ACS Nano, 7*, 5577–5587. https://doi.org/10.1021/nn401856u

Chen, C., Wang, S., Wang, J., Yao, F., Tang, X., & Guo, W. (2023). Nanosized drug delivery strategies in osteosarcoma chemotherapy. *APL Bioengineering, 7*(1), Article 011501. https://doi.org/10.1063/5.0137026

Chen, E. I., & Yates, J. R. (2006). Maspin and tumor metastasis. *IUBMB Life, 58*(1), 25–29. https://doi.org/10.1080/15216540500531721

D'Souza, S (2014). A review of in vitro drug release test methods for nano-sized dosage forms. *Advances in Pharmaceutics*. https://doi.org/10.1155/2014/304757, 304757.

da Silva Santos, N. P., Nascimento, S. C., Wanderley, M. S., Pontes-Filho, N. T., da Silva, J. F., de Castro, C. M., Pereira, E. C., da Silva, N. H., Honda, N. K., & Santos-Magalhães, N. S. (2006). Nanoencapsulation of usnic acid: An attempt to improve antitumour activity and reduce hepatotoxicity. *European Journal Of Pharmaceutics And Biopharmaceutics, 64*(2), 154–160. https://doi.org/10.1016/j.ejpb.2006.05.018

Dimiou, S., McCabe, J., Booth, R., Booth, J., Nidadavole, K., Svensson, O., Sparén, A., Lindfors, L., Paraskevopoulou, V., Mead, H., Coates, L., Workman, D., Martin, D., Treacher, K., Puri, S., Taylor, L. S., & Yang, B. (2023). Selecting counterions to

improve ionized hydrophilic drug encapsulation in polymeric nanoparticles. *Molecular Pharmaceutics, 20*(2), 1138–1155. https://doi.org/10.1021/acs.molpharmaceut.2c00855

Dou, T., Wang, J., Han, C., Shao, X., Zhang, J., & Lu, W. (2019). Cellular uptake and transport characteristics of chitosan modified nanoparticles in Caco-2 cell monolayers. *International Journal Of Biological Macromolecules, 138*, 791–799. https://doi.org/10.1016/j.ijbiomac.2019.07.168

Du, G., Belić, D., Del Giudice, A., Alfredsson, V., Carnerup, A. M., Zhu, K., Nyström, B., Wang, Y., Galantini, L., & Schillén, K. (2022). Condensed supramolecular helices: The twisted sisters of DNA. *Angewandte Chemie, 134*, Article e202113279. https://doi.org/10.1002/anie.202113279

Dyawanapelly, S., Koli, U., Dharamdasani, V., Jain, R., & Dandekar, P. (2016). Improved mucoadhesion and cell uptake of chitosan and chitosan oligosaccharide surface-modified polymer nanoparticles for mucosal delivery of proteins. *Drug Delivery And Translational Research, 6*(4), 365–379. https://doi.org/10.1007/s13346-016-0295-x

Francolini, I., Giansanti, L., Piozzi, A., Altieri, B., Mauceri, A., & Mancini, G. (2019b). Glucosylated liposomes as drug delivery systems of usnic acid to address bacterial infections. *Colloids and Surfaces. B, Biointerfaces, 181*, 632–638. https://doi.org/10.1016/j.colsurfb.2019.05.056

Francolini, I., Norris, P., Piozzi, A., Donelli, G., & Stoodley, P. (2004). Usnic acid, a natural antimicrobial agent able to inhibit bacterial biofilm formation on polymer surfaces. *Antimicrobial Agents And Chemotherapy, 48*(11), 4360–4365. https://doi.org/10.1128/AAC.48.11.4360-4365.2004

Francolini, I., Perugini, E., Silvestro, I., Lopreiato, M., Scotto d'Abusco, A., Valentini, F., Placidi, E., Arciprete, F., Martinelli, A., & Piozzi, A. (2019a). Graphene oxide oxygen content affects physical and biological properties of scaffolds based on chitosan/graphene oxide conjugates. *Materials, 12*(7), 1142. https://doi.org/10.3390/ma12071142

Francolini, I., Taresco, V., Crisante, F., Martinelli, A., D'Ilario, L., & Piozzi, A (2013). Water soluble usnic acid-polyacrylamide complexes with enhanced antimicrobial activity against *Staphylococcus epidermidis*. *International Journal Of Molecular Sciences, 14*(4), 7356–7369. https://doi.org/10.3390/ijms14047356

Grumezescu, A. M., Cotar, A. I., Andronescu, E., Ficai, A., Ghitulica, C. D., Grumezescu, V., Vasile, B. S., & Chifiriuc, M. C. (2013). In vitro activity of the new water-dispersible Fe3O4@ usnic acid nanostructure against planktonic and sessile bacterial cells. *Journal of Nanoparticle Research, 15*, 1766–1776. https://doi.org/10.1007/s11051-013-1766-3

Guadarrama-Escobar, O. R., Serrano-Castañeda, P., Anguiano-Almazán, E., Vázquez-Durán, A., Peña-Juárez, M. C., Vera-Graziano, R., Morales-Florido, M. I., Rodriguez-Perez, B., Rodriguez-Cruz, I. M., Miranda-Calderón, J. E., & Escobar-Chávez, J. J. (2023). Chitosan nanoparticles as oral drug carriers. *International Journal of Molecular Sciences, 24*(5), 4289. https://doi.org/10.3390/ijms24054289

Hare, J. I., Lammers, T., Ashford, M. B., Puri, S., Storm, G., & Barry, S. T. (2017). Challenges and strategies in anti-cancer nanomedicine development: An industry perspective. *Advanced Drug Delivery Reviews, 108*, 25–38. https://doi.org/10.1016/j.addr.2016.04.025

Ingólfsdóttir, K. (2002). Usnic acid. *Phytochemistry, 61*(7), 729–736. https://doi.org/10.1016/S0031-9422(02)00383-7

Isakoff, M. S., Bielack, S. S., Meltzer, P., & Gorlick, R. (2015). Osteosarcoma: Current treatment and a collaborative pathway to success. *Journal of Clinical Oncology: Official Journal Of The American Society of Clinical Oncology, 33*(27), 3029–3035. https://doi.org/10.1200/JCO.2014.59.4895

Jacob, P. L., Ruiz Cantu, L. A., Pearce, A. K., He, Y., Lentz, J. C., Moore, J. C., Machado, F., Rivers, G., Apebende, E., Fernandez, M. R., Francolini, I., Wildman, R., Howdle, S. M., & Taresco, V. (2021). Poly (glycerol adipate) (PGA) backbone modifications with a library of functional diols: Chemical and physical effects. *Polymer, 228*, Article 123912. https://doi.org/10.1016/j.polymer.2021.123912

Jin, J., Rao, Y., Bian, X., Zeng, A., & Yang, G. (2013). Solubility of (+)-usnic acid in water, ethanol, acetone, ethyl acetate and n-hexane. *Journal of Solution Chemistry, 42*(5), 1018–1027. https://doi.org/10.1007/s10953-013-0010-1

Kalaydina, R. V., Bajwa, K., Qorri, B., Decarlo, A., & Szewczuk, M. R. (2018). Recent advances in "smart" delivery systems for extended drug release in cancer therapy. *International Journal Of Nanomedicine, 13*, 4727–4745. https://doi.org/10.2147/IJN.S168053

Kansara, M., Teng, M. W., Smyth, M. J., & Thomas, D. M. (2014). Translational biology of osteosarcoma. *Nature Reviews Cancer, 14*(11), 722–735. https://doi.org/10.1038/nrc3838

Khan, F., Yu, H., & Kim, Y. M. (2020). Bactericidal Activity of usnic acid-chitosan nanoparticles against persister cells of biofilm-forming pathogenic bacteria. *Marine Drugs, 18*(5), 270. https://doi.org/10.3390/md18050270

Koppel, D. E. (1972). Analysis of macromolecular polydispersity in intensity correlation spectroscopy: The method of cumulants. *The Journal of Chemical Physics, 57*(11), 4814–4820. https://doi.org/10.1063/1.1678153

Körpe, D. A., Malekghasemi, S., Aydın, U., & Duman, M. (2014). Fabrication of monodispersive nanoscale alginate–chitosan core–shell particulate systems for controlled release studies. *Journal of Nanoparticle Research, 16*(12), 2754. https://doi.org/10.1007/s11051-014-2754-y

Krajka-Kuźniak, V., Paluszczak, J., Kleszcz, R., & Baer-Dubowska, W. (2021). (+)-Usnic acid modulates the Nrf2-ARE pathway in FaDu hypopharyngeal carcinoma cells. *Molecular and Cellular Biochemistry, 476*(6), 2539–2549. https://doi.org/10.1007/s11010-021-04092-7

Kumar, S., Dutta, J., & Dutta, P. K. (2009). Preparation and characterization of N-heterocyclic chitosan derivative based gels for biomedical applications. *International Journal Of Biological Macromolecules, 45*(4), 330–337. https://doi.org/10.1016/j.ijbiomac.2009.08.002

Kwong, S. P., & Wang, C. (2020). Review: Usnic acid-induced hepatotoxicity and cell death. *Environmental Toxicology And Pharmacology, 80*, Article 103493. https://doi.org/10.1016/j.etap.2020.103493

Lawson, C. L., & Hanson, R. J. (1974). *Solving Least Squares Problems*. Englewood Cliffs, NJ: Prentice Hall. https://doi.org/10.1007/978-1-4612-3468-5_5

Li, S., Xiong, Y., & Zhang, X. (2017). Poloxamer surface modified trimethyl chitosan nanoparticles for the effective delivery of methotrexate in osteosarcoma. *Biomedicine & pharmacotherapy, 90*, 872–879. https://doi.org/10.1016/j.biopha.2017.04.004

Li, S., Zhang, H., Liu, J., & Shang, G. (2023). Targeted therapy for osteosarcoma: a review. *Journal of Cancer Research And Clinical Oncology*. https://doi.org/10.1007/s00432-023-04614-4

Lilienthal, I., & Herold, N. (2020). Targeting molecular mechanisms underlying treatment efficacy and resistance in osteosarcoma: A review of current and future strategies. *International Journal Of Molecular Sciences, 21*(18), 6885. https://doi.org/10.3390/ijms21186885

Lira, M. C., Siqueira-Moura, M. P., Rolim-Santos, H. M., Galetti, F. C., Simioni, A. R., Santos, N. P., Tabosa Do Egito, E. S., Silva, C. L., Tedesco, A. C., & Santos-Magalhães, N. S. (2009). In vitrouptake and antimycobacterial activity of liposomal usnic acid formulation. *Journal of Liposome Research, 19*(1), 49–58. https://doi.org/10.1080/08982100802564628

Luzina, O. A., & Salakhutdinov, N. F. (2018). Usnic acid and its derivatives for pharmaceutical use: a patent review (2000-2017). *Expert Opinion On Therapeutic Patents, 28*(6), 477–491. https://doi.org/10.1080/13543776.2018.1472239

Machowska, M., Wachowicz, K., Sopel, M., & Rzepecki, R. (2014). Nuclear location of tumor suppressor protein Maspin inhibits proliferation of breast cancer cells without affecting proliferation of normal epithelial cells. *BMC Cancer, 14*, 142. https://doi.org/10.1186/1471-2407-14-142

Maleki, Dana P., Hallajzadeh, J., Asemi, Z., Mansournia, M. A., & Yousefi, B (2021). Chitosan applications in studying and managing osteosarcoma. *International Journal Of Biological Macromolecules, 169*, 321–329. https://doi.org/10.1016/j.ijbiomac.2020.12.058

Martinelli, A., Bakry, A., D'Ilario, L., Francolini, I., Piozzi, A., & Taresco, V. (2014). Release behavior and antibiofilm activity of usnic acid-loaded carboxylated poly(L-lactide) microparticles. *European Journal Of Pharmaceutics And Biopharmaceutics, 88*(2), 415–423. https://doi.org/10.1016/j.ejpb.2014.06.002

Meng, Q., Zhong, S., Xu, L., Wang, J., Zhang, Z., Gao, Y., & Cui, X. (2022). Review on design strategies and considerations of polysaccharide-based smart drug delivery systems for cancer therapy. *Carbohydrate Polymers, 279*, Article 119013. https://doi.org/10.1016/j.carbpol.2021.119013

Modi, S., & Anderson, B. D. (2013). Determination of drug release kinetics from nanoparticles: overcoming pitfalls of the dynamic dialysis method. *Molecular Pharmaceutics, 10*(8), 3076–3089. https://doi.org/10.1021/mp400154a

Mohammed, M. A., Syeda, J. T. M., Wasan, K. M., & Wasan, E. K. (2017). An overview of chitosan nanoparticles and its application in non-parenteral drug delivery. *Pharmaceutics, 9*(4), 53. https://doi.org/10.3390/pharmaceutics9040053

Nguyen, D. D., & Lai, J.-Y. (2022). Synthesis, bioactive properties, and biomedical applications of intrinsically therapeutic nanoparticles for disease treatment. *Chemical Engineering Journal, 435*(2), Article 134970. https://doi.org/10.1016/j.cej.2022.134970

Nguyen, D. D., Yao, C.-H., Lue, S. J., Yang, C.-J., Su, Y.-H., Huang, C.-C., & Lai, J.-Y. (2023). Amination-mediated nano eye-drops with enhanced corneal permeability and effective burst release for acute glaucoma treatment. *Chemical Engineering Journal, 451*(1), Article 138620. https://doi.org/10.1016/j.cej.2022.138620

Oh, E., Wang, W., Park, K. H., Park, C., Cho, Y., Lee, J., Kang, E., & Kang, H. (2022). (+)-Usnic acid and its salts, inhibitors of SARS-CoV-2, identified by using in silico methods and in vitro assay. *Scientific reports, 12*(1), 13118. https://doi.org/10.1038/s41598-022-17506-3

Pedroso-Santana, S., & Fleitas-Salazar, N. (2020). Ionotropic gelation method in the synthesis of nanoparticles/microparticles for biomedical purposes. *Polymer International, 69*(5), 443–447. https://doi.org/10.1002/pi.5970

Popovici, V., Matei, E., Cozaru, G. C., Bucur, L., Gîrd, C. E., Schröder, V., Ozon, E. A., Sarbu, I., Musuc, A. M., Atkinson, I., Rusu, A., Petrescu, S., Mitran, R. A., Anastasescu, M., Caraiane, A., Lupuliasa, D., Aschie, M., & Badea, V. (2022). Formulation and development of bioadhesive oral films containing *Usnea barbata* (L.) F.H. wigg dry ethanol extract (F-UBE-HPC) with antimicrobial and anticancer properties for potential use in oral cancer complementary therapy. *Pharmaceutics, 14*(9), 1808. https://doi.org/10.3390/pharmaceutics14091808

Pyrczak-Felczykowska, A., Reekie, T. A., Jąkalski, M., Hać, A., Malinowska, M., Pawlik, A., Ryś, K., Guzow-Krzemińska, B., & Herman-Antosiewicz, A. (2022). The isoxazole derivative of usnic acid induces an ER stress response in breast cancer cells that leads to paraptosis-like cell death. *International Journal Of Molecular Sciences, 23*(3), 1802. https://doi.org/10.3390/ijms23031802

Rasool, M., Malik, A., Waquar, S., Arooj, M., Zahid, S., Asif, M., Shaheen, S., Hussain, A., Ullah, H., & Gan, S. H. (2022). New challenges in the use of nanomedicine in cancer therapy. *Bioengineered, 13*(1), 759–773. https://doi.org/10.1080/21655979.2021.2012907

Rauschenbach, M., Lawrenson, S. B., Taresco, V., Pearce, A. K., & O'Reilly, R. K (2020). Antimicrobial hyperbranched polymer–usnic acid complexes through a combined ROP-RAFT strategy. *Macromolecular Rapid Communication, 41*, Article 2000190. https://doi.org/10.1002/marc.202000190

Ritger, P. L., & Peppas, N. A. (1987). A simple equation for description of solute release I. Fickian and non-fickian release from non-swellable devices in the form of slabs, spheres, cylinders or discs. *Journal of controlled release, 5*, 23–36. https://doi.org/10.1016/0168-3659(87)90034-4

Sharma, M., Sharma, R., Jain, D. K., & Saraf, A. (2019). Enhancement of oral bioavailability of poorly water soluble carvedilol by chitosan nanoparticles:

Optimization and pharmacokinetic study. *International Journal of Biological Macromolecules, 135*, 246–260. https://doi.org/10.1016/j.ijbiomac.2019.05.162

Sheng, J., Han, L., Qin, J., Ru, G., Li, R., Wu, L., Cui, D., Yang, P., He, Y., & Wang, J. (2015). N-trimethyl chitosan chloride-coated PLGA nanoparticles overcoming multiple barriers to oral insulin absorption. *ACS Applied Materials & Interfaces, 7*(28), 15430–15441. https://doi.org/10.1021/acsami.5b03555

Siepmann, J., & Peppas, N. A. (2011). Higuchi equation: derivation, applications, use and misuse. *International Journal Of Pharmaceutics, 418*(1), 6–12. https://doi.org/10.1016/j.ijpharm.2011.03.051

Silvestro, I., Francolini, I., Di Lisio, V., Martinelli, A., Pietrelli, L., Scotto d'Abusco, A., Scoppio, A., & Piozzi, A. (2020b). Preparation and characterization of TPP-chitosan crosslinked scaffolds for tissue engineering. *Materials, 13*(16), 3577. https://doi.org/10.3390/ma13163577

Silvestro, I., Lopreiato, M., Scotto d'Abusco, A., Di Lisio, V., Martinelli, A., Piozzi, A., & Francolini, I. (2020a). Hyaluronic acid reduces bacterial fouling and promotes fibroblasts' adhesion onto chitosan 2d-wound dressings. *International Journal Of Molecular Science, 21*(6), 2070. https://doi.org/10.3390/ijms21062070

Silvestro, I., Sergi, R., Scotto d'Abusco, A., Mariano, A., Martinelli, A., Piozzi, A., & Francolini, I. (2021). Chitosan scaffolds with enhanced mechanical strength and elastic response by combination of freeze gelation, photo-crosslinking and freeze-drying. *Carbohydrate Polymers, 267*, Article 118156. https://doi.org/10.1016/j.carbpol.2021.118156

Stiernagle, T. (2006). Maintenance of C. elegans. *The C. elegans Research Community, WormBook*. PasadenaCA: WormBook. https://doi.org/10.1895/wormbook.1.101.1

Taresco, V., Francolini, I., Padella, F., Bellusci, M., Boni, A., Innocenti, C., Martinelli, A., D'Ilario, L., & Piozzi, A. (2015b). Design and characterization of antimicrobial usnic acid loaded-core/shell magnetic nanoparticles. *Materials Science & Engineering. C, Materials for Biological Applications, 52*, 72–81. https://doi.org/10.1016/j.msec.2015.03.044

Taresco, V., Gontrani, L., Crisante, F., Francolini, I., Martinelli, A., D'Ilario, L., Bordi, F., & Piozzi, A (2015a). Self-Assembly of catecholic moiety-containing cationic random acrylic copolymers. *The Journal Of Physical Chemistry. B, 119*(26), 8369–8379. https://doi.org/10.1021/acs.jpcb.5b05022

Taresco, V., Tulini, I., Francolini, I., & Piozzi, A. (2022). Polyglycerol adipate-grafted polycaprolactone nanoparticles as carriers for the antimicrobial compound usnic acid. *International Journal Of Molecular Sciences, 23*(22), 14339. https://doi.org/10.3390/ijms232214339

Tasca, E., Andreozzi, P., Del Giudice, A., Galantini, L., Schillén, K., Maria Giuliani, A., … Giustini, M. (2020). Poloxamer/sodium cholate co-formulation for micellar encapsulation of doxorubicin with high efficiency for intracellular delivery: An in-vitro bioavailability study. *Journal of Colloid and Interface Science, 579*, 551–561. https://doi.org/10.1016/j.jcis.2020.06.096

Tavares, J. K., Ulson de Souza, A. A., José Vladimir de Oliveira, J., Priamo, W. L., & Guelli Ulson de Souza, S. M. A. (2016). Modeling of the controlled release of betacarotene into anhydrous ethanol from microcapsules. *OpenNano, 1*, 25–35. https://doi.org/10.1016/j.onano.2016.05.001

Tripathi, A. H., Negi, N., Gahtori, R., Kumari, A., Joshi, P., Tewari, L. M., Joshi, Y., Bajpai, R., Upreti, D. K., & Upadhyay, S. K. (2022). A Review of anti-cancer and related properties of lichen-extracts and metabolites. *Anti-cancer Agents In Medicinal Chemistry, 22*(1), 115–142. https://doi.org/10.2174/1871520621666210322094647

Tscharnuter, W. W. (2001). Mobility measurements by phase analysis. *Appl. Opt., 40*(24), 3995–4003.

Venditti, I., Iucci, G., Fratoddi, I., Cipolletti, M., Montalesi, E., Marino, M., Secchi, V., & Battocchio, C. (2020). Direct conjugation of resveratrol on hydrophilic gold nanoparticles: Structural and cytotoxic studies for biomedical applications. *Nanomaterials, 10*(10), 1898. https://doi.org/10.3390/nano10101898

Wang, H., Xuan, M., Huang, C., & Wang, C. (2022). Advances in research on bioactivity, toxicity, metabolism, and pharmacokinetics of usnic acid in vitro and in vivo. *Molecules, 27*(21), 7469. https://doi.org/10.3390/molecules27217469

Wang, Y., Li, P., Tran, T. T.-D., Zhang, J., & Kong, L. (2016). Manufacturing techniques and surface engineering of polymer based nanoparticles for targeted drug delivery to cancer. *Nanomaterials, 6*, 26. https://doi.org/10.3390/nano6020026

Yang, Y., Nguyen, T. T., Jeong, M. H., Crişan, F., Yu, Y. H., Ha, H. H., Choi, K. H., Jeong, H. G., Jeong, T. C., Lee, K. Y., Kim, K. K., Hur, J. S., & Kim, H. (2016). Inhibitory activity of (+)-usnic acid against non-small cell lung cancer cell motility. *PloS One, 11*(1), Article e0146575. https://doi.org/10.1371/journal.pone.0146575